© 2016 IJSRSET | Volume 2 | Issue 2 | Print ISSN : 2395-1990 | Online ISSN : 2394-4099
Themed Section: Engineering and Technology

Electrochemical Corrosion Behavior, Microstructure, Mechanical and Thermal Performance of Tin-Aluminum Based Bearing Alloys

Abu Bakr El-Bediwi[1], N. A. El-Shishtawi[1], Manal Mawloud Abdullah[1, 2]

[1]Metal Physics Lab., Physics Department, Faculty of Science, Mansoura University, Egypt
[1, 2] Faculty of Education Aboaesa, University of Alzawya, Libya

ABSTRACT

Electrochemical corrosion behavior, elastic modului, internal friction, Vickers hardness, thermal performance and microstructure of $Sn_{80}Al_{20}$, $Sn_{70}Al_{20}Bi_5Zn_3Cu_2$, $Sn_{65}Al_{20}Sb_5Pb_5Cd_5$, $Sn_{70}Al_{20}Sb_5Ag_3Zn_2$ and $Sn_{63}Al_{20}Sb_{10}Pb_5Zn_2$ alloys have been investigated. Internal friction of $Sn_{80}Al_{20}$ alloy decreased after adding Bi- Zn- Cu or Sb- Pb- Cd or Sb- Ag- Zn or Sb- Pb- Zn elements. Elastic modulus and lattice microstrain of $Sn_{80}Al_{20}$ alloy decreased after adding Bi- Zn- Cu or Sb- Pb- Cd or Sb- Ag- Zn but it's increased after adding 10%Sb- 5%Pb- 2%Zn. Vickers hardness of $Sn_{80}Al_{20}$ alloy varied after adding Bi- Zn- Cu or Sb- Pb- Cd or Sb- Ag- Zn or Sb- Pb- Zn elements. The corrosion rate of $Sn_{80}Al_{20}$ alloy in 0.5 M HCl increased after adding Bi- Zn-Cu or Sb- Ag- Zn or Sb- Pb- Zn elements but it's decreased after Sb-Pb-Cd elements. The corrosion current density (icorr) of $Sn_{80}Al_{20}$ alloy in 0.5 M HCl increased after adding Bi- Zn-Cu or Sb- Pb- Cd or Sb- Pb- Zn elements but it's decreased after Sb-Ag-Zn elements. The $Sn_{70}Al_{20}Sb_5Ag_3Zn_2$ alloy has the beast properties for bearing applications.

Key words: Corrosion Parameters, Microstructure, Elastic Modulus, Internal Friction, Vickers Hardness, Thermal Behavior

I. INTRODUCTION

Bearings are used as a mechanical component to transfer the power and to move a certain part which makes them rotate easily. It can be classified into two major groups, sliding bearings and rolling bearings, depending on their friction type. Bearings are used to prevent friction between parts during relative movement. Tin-based bearing alloys with different compositions is widely used in the automotive industry and especially in heavy industrial service conditions [1]. High tin- aluminum alloys are used as linings bonded to a steel-backing strip. Aluminum- tin alloys have good mechanical properties with conformability but these are quite costly. Al-Sn alloys have a very long history to be used as bearing materials [2]. Also Al-Sn alloys deliver a good combination of strength and surface properties [3]. Low modulus of elasticity is required in a bearing alloy to ensure good compatibility with the journal surface. Aluminum has a low modulus of elasticity. Indium and lead have the lowest modulus of elasticity of all the soft phases alloying with aluminum [4]. The fatigue strength of cold worked and heat treated $AlSn_{20}Cu_1$ alloy having reticular structure is close to that of $CuPb_{30}$ alloy with higher seizure resistance [5]. Aluminum- tin based alloys are widely used as sliding bearing materials in automobile and shipbuilding industry [6, 7]. Tin phase in Al-Sn bearing materials can provide suitable friction properties and shear surface during sliding because it's low modulus, low strength and the excellent anti-welding characteristics with iron [6]. Two compositions of aluminum base alloys were selected and equal amounts of tin and lead as a soft phase were prepared by impeller mixing and chill casting technique [8]. Aluminum- tin and lead- aluminum alloys slightly differ in mechanical properties. Adding Ag or Au to $SnSb_5$ alloy reduced the melting temperature and increased the capabilities for precipitation hardening [9]. But strength and ductility of $SnSb_5$ alloy improved after adding Bi or Cu content [10]. Elastic modulus and internal friction of $Sn_{86}Sb_{10}Cu_2X_2$ (X = Pb or Ag or Se or Cd- Zn) alloys dependent on alloy composition [11]. The influence of

adding Cu or Ag or Cu- Ag on structure, electrical resistivity and elastic modulus of $SnSb_7$ alloy has been investigated [12]. The $SnSb_7Ag_2Cu_2$ has best bearing properties such as lowest internal friction, cast and adequate elastic modulus. Adding 1 wt. % Cu or Ag improved mechanical properties of Sn-Sb alloy [13]. Adding Bi or Cu to $SnSb_5$ alloy increased both ultimate tensile strength (UTS) and ductility [14]. Adding (Cu-Pb) to Sn-Sb alloy improves their elastic modulus, internal friction, hardness and thermal conductivity [15]. The aim of this research was to investigate the modification structure by adding different alloying elements on electrochemical corrosion behavior, hardness, elastic modulus, internal friction and thermal performance of tin-aluminum based alloy

II. METHODS AND MATERIAL

Were melted in a muffle furnace using tin, aluminum, bismuth, zinc, copper, lead, antimony, sliver and cadmium of purity better than 99.5 %. The resulting ingots were turned and re-melted four times to increase the homogeneity. Long ribbons of ~ 4 mm width and ~80 μm thickness were prepared by melt spinning technique. The surface velocity of the roller was 31.4 m/s giving a cooling rate of ~3.7×10^5 K/s. The samples then cut into convenient shape for the measurements using double knife cuter. Microstructure of used samples was performed using scanning electron microscope (JEOL JSM-6510LV, Japan) and Shimadzu X–ray Diffractometer (Dx–30, Japan) of Cu–Kα radiation with λ=1.54056 Å at 45 kV and 35 mA and Ni–filter in the angular range 2θ ranging from 0 to 100° in continuous mode with a scan speed 5 deg/min. The differential thermal analysis (DSC) thermographs were obtained by SDT Q600 (V20.9 Build 20) instrument (U. S. A) with heating rate 10 k/min in the temperature range 50-400 °C. All the samples have the same mass, which is 2 mg. A digital Vickers micro-hardness tester, (Model-FM-7- Japan), was used to measure Vickers hardness values. The internal friction Q^{-1} and the elastic constants were determined using the dynamic resonance method. The value of the dynamic Young modulus *E* is determined by the relationship [16– 18]. Electrochemical corrosion measurements of used alloys were performed using Gamry Instrument PCI4G750 Potentiostat/Galvanostat/ZRA.

III. RESULTS AND DISCUSSION

A. Microstructure

X-ray diffraction patterns of $Sn_{70}Al_{20}Bi_5Zn_3Cu_2$ alloy have lines corresponding to tetragonal tin phase, hexagonal bismuth phase and face centered cubic aluminum phase. Copper and zinc atoms dissolved in matrix alloy. Also started base a round 180 counts, that is mean that, the matrix atoms random distribution in small part as shown in Figure 1a. Figure 1b shows x-ray diffraction patterns of $Sn_{65}Al_{20}Sb_5Pb_5Cd_5$ alloy which have lines corresponding to tetragonal tin phase, face centered cubic lead phase, antimony phase and face centered cubic aluminum phase. Cadmium atoms dissolved in matrix alloy. Also started base a round 230 counts, that is mean that, the matrix atoms random distribution in small part. X-ray diffraction patterns of $Sn_{70}Al_{20}Sb_5Ag_3Zn_2$ alloy have lines corresponding to tetragonal tin phase, zinc phase, silver phase sliver-antimony intermetallic phase and face centered cubic aluminum phase. Also started base a round 180 counts, that is mean that, the matrix atoms random distribution in small part as shown in Figure 1c. X-ray diffraction patterns of $Sn_{63}Al_{20}Sb_{10}Pb_5Zn_2$ alloy have lines corresponding to tetragonal tin phase, lead phase, antimony phase and face centered cubic aluminum phase. Zinc atoms dissolved in alloy matrix. Also started base a round 100 counts, that is mean that, the matrix atoms random distribution in small part as shown in Figure 1d. X-ray diffraction analysis in Table 1 (a, b, c and d) show that adding different ternary alloying elements, Bi- Zn-Cu or Sb- Pb- Cd or Sb- Ag- Zn or Sb- Pb- Zn, to $Sn_{80}Al_{20}$ alloy caused a change in matrix microstructure such as peak intensity (crystallinity), peak broadness (crystal size), peak position (orientation) and started base line (amorphousity).

Lattice parameters and unit cell volume of body centered tetragonal tin in penta tin-aluminum based alloys are determined using equation [16] and then listed in Table 2. The volume of tetragonal unit cell is a^2c.

The estimated crystal size is given by Scherer equation [16] and then listed in Table 2. Also from the relation between full width half maximum (β) and 4tanθ as shown in Figure 2, the induced internal lattice microstrain of $Sn_{80}Al_{20}$, $Sn_{70}Al_{20}Bi_5Zn_3Cu_2$, $Sn_{65}Al_{20}Sb_5Pb_5Cd_5$, $Sn_{70}Al_{20}Sb_5Ag_3Zn_2$, and

$Sn_{63}Al_{20}Sb_{10}Pb_5Zn_2$ alloys were calculated and then listed Table 3.

The results show that, lattice parameters, unit volume cell, crystal size and lattice microstrain of $Sn_{80}Al_{20}$ alloy changed after adding ternary alloying elements, Bi- Zn- Cu or Sb- Pb- Cd or Sb- Ag- Zn or Sb- Pb- Zn which confirmed that there is a change in alloy matrix microstructure.

Scanning electron micrographs analysis

Scanning electron micrograph of $Sn_{70}Al_{20}Bi_5Zn_3Cu_2$ alloy, Figure 3a, shows tin matrix with different grain size, white spherical particles of aluminum and different area contain a mixed tin-aluminum-zinc-copper as a circular with different shape and size in matrix alloy. Also different line dislocation appeared in matrix. Scanning electron micrograph of $Sn_{65}Al_{20}Sb_5Pb_5Cd_5$ alloy, Figure 3b, shows disturbed aluminum grains of different size and orientation in tin matrix with small dissolved particles (Sb or Pb or Cd) disturbed in matrix. Scanning electron micrograph of $Sn_{70}Al_{20}Sb_5Ag_3Zn_2$ alloy, Figure 3c, shows a lamellar tin structure which has different size, shape and orientation contain aluminum grains and small particles (Sb or Ag or Zn) dissolved in matrix. Scanning electron micrograph of $Sn_{63}Al_{20}Sb_{10}Pb_5Zn_2$ alloy, Figure 3d, shows a dendrite tin structure which has different size, shape and orientation of aluminum grains and small particles (Sb or Pb or Zn) dissolved in matrix.

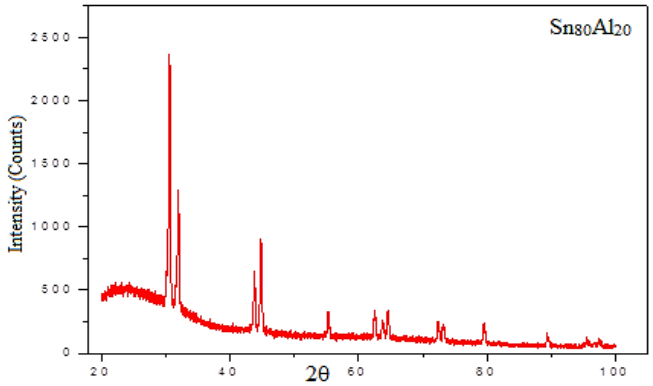

Figure 1a:- X-ray diffraction patterns of $Sn_{80}Al_{20}$ alloy

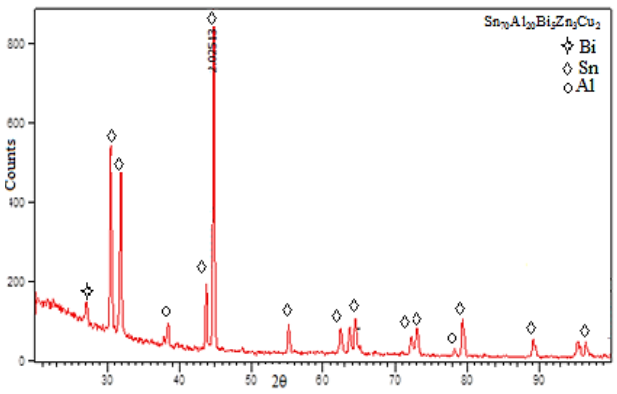

Figure 1b:- x-ray diffraction patterns of $Sn_{70}Al_{20}Bi_5Zn_3Cu_2$ alloy

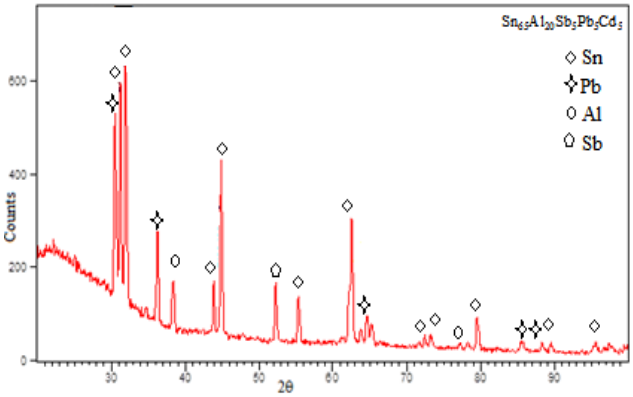

Figure 1c:- X-ray diffraction patterns of $Sn_{65}Al_{20}Sb_5Pb_5Cd_5$ alloy

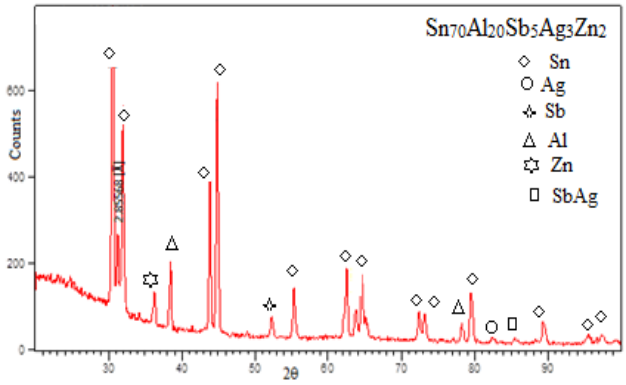

Figure 1d:-X-ray diffraction patterns of $Sn_{70}Al_{20}Sb_5Ag_3Zn_2$ alloy

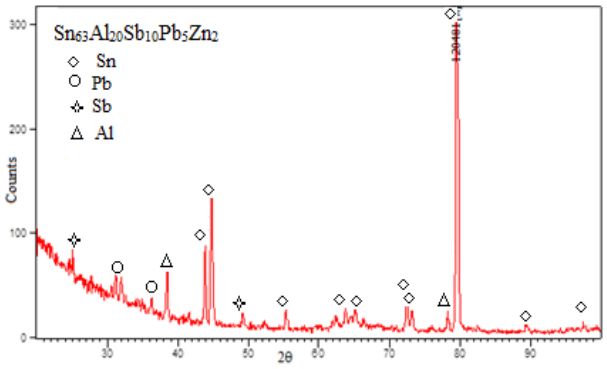

Table 1a:- x-ray diffraction analysis of $Sn_{70}Al_{20}Bi_5Zn_3Cu_2$ alloy

2θ	d Å	Int. %	FHWM	Area	Phase	hkl
27.203	3.278	7.01	0.24	12.7	Bi	012
30.477	2.933	55.7	0.26	108.99	Sn	200
31.942	2.802	51.94	0.256	101.65	Sn	101
37.79	2.381	4.57	0.001	0.02	Bi	104
38.375	2.346	7.12	0.315	17.15	Al	111
43.803	2.067	20.74	0.256	40.59	Sn	220
44.752	2.025	100	0.256	195.7	Sn	211
55.21	1.664	8.92	0.197	13.43	Sn	301
62.357	1.489	7.54	0.177	10.21	Sn	112
63.748	1.46	7.81	0.276	16.46	Sn	400
64.392	1.447	11.12	0.236	20.08	Sn	321
65.21	1.431	1.68	0.09	1.17	Sn	420
72.284	1.307	5.3	0.236	9.58	Sn	420
73.017	1.296	9.08	0.276	19.14	Sn	411
78.268	1.222	2.16	0.315	5.19	Al	311
79.339	1.208	11.43	0.197	17.21	Sn	312
89.158	1.098	5.27	0.315	12.7	Sn	431
95.343	1.043	4.6	0.236	8.31	Sn	332
96.43	1.033	3.97	0.288	11.81	Sn	440

Table 1b:- x-ray diffraction analysis of $Sn_{65}Al_{20}Sb_5Pb_5Cd_5$ alloy

2θ	d Å	Int. %	FHWM	Area	Phase	hkl
30.54	2.923	64.31	0.177	70.54	Sn	200
31.28	2.86	75.84	0.256	120.17	Pb	111
32.04	2.794	100	0.236	146.25	Sn	101
36.196	2.482	29.09	0.295	53.17	Pb	200
38.41	2.344	17.54	0.315	34.19	Al	111
43.865	2.064	18.35	0.236	26.84	Sn	220
44.89	2.019	60.32	0.256	95.56	Sn	211
52.27	1.75	20.16	0.236	29.48	Sb	[202]
55.32	1.661	14.66	0.177	16.08	Sn	301
62.51	1.486	41.78	0.157	40.74	Sn	112
63.815	1.459	4.33	0.236	6.33	Sn	400
64.543	1.444	9.12	0.177	10	Sn	321
65.295	1.429	6.63	0.315	12.93	Sn	420
72.43	1.305	3.79	0.236	5.54	Sn	420
73.2	1.293	4.36	0.394	10.63	Sn	411
78.25	1.222	2.14	0.472	6.27	Al	311
79.489	1.206	10.24	0.157	9.98	Sn	312
85.47	1.136	3.16	0.394	7.71	Pb	331
88.368	1.106	2.73	0.472	7.98	Pb	420
89.44	1.096	3.07	0.315	5.99	Sn	431
95.504	1.041	3.32	0.768	21.34	Sn	332

Table 1c:- x-ray diffraction analysis of $Sn_{70}Al_{20}Sb_5Ag_3Zn_2$ alloy

2θ	d Å	Int. %	FHWM	Area	Phase	hkl
30.62	2.92	100	0.295	199.49	Sn	200
31.32	2.86	24.4	0.236	38.95	Sn	200
32.02	2.795	68.69	0.276	127.89	Sn	101
36.27	2.477	10.78	0.315	22.93	Zn	002
38.45	2.34	22.8	0.236	36.38	Al	111
43.81	2.067	50.55	0.177	60.51	Sn	220
44.9	2.02	84.15	0.276	156.68	Sn	211
52.22	1.752	6.22	0.315	13.24	Sb	[202]
55.25	1.663	14.72	0.236	23.5	Sn	301
62.53	1.485	23.16	0.157	24.64	Sn	112
63.75	1.46	8.72	0.276	16.24	Sn	400
64.555	1.444	20.82	0.177	24.92	Sn	321
72.421	1.305	9.02	0.315	19.19	Sn	420
73.12	1.29	8.82	0.35	21.13	Sn	411
78.231	1.22	5.91	0.47	18.86	Al	311
79.47	1.206	16.38	0.197	21.78	Sn	312
82.477	1.17	1.58	0.47	5.06	Ag	222
85.582	1.135	1.33	0.47	4.23	SbAg	042
89.307	1.097	7.08	0.197	9.42	Sn	431
95.551	1.041	3.08	0.63	13.11	Sn	103
97.45	1.025	2.64	0.576	13.88	Sn	521

Table 1d: - x-ray diffraction analysis of $Sn_{63}Al_{20}Sb_{10}Pb_5Zn_2$ alloy

2θ	d Å	Int. %	FHWM	Area	Phase	hkl
25.098	3.548	17.03	0.385	13.14	Sb	[101]
31.25	2.862	7.62	0.236	5.34	Pb	111
32.039	2.794	7.55	0.315	7.06	Sn	101
36.267	2.477	8.43	0.039	0.67	Zn	002
38.48	2.34	16.2	0.197	9.47	Al	111
43.95	2.060	22.81	0.197	13.33	Sn	220
44.90	2.019	39.14	0.276	32.02	Sn	211
49.267	1.85	3.6	0.47	5.04	Sb	006
55.33	1.66	6.3	0.315	5.9	Sn	301
62.526	1.486	2.75	0.947	7.7	Sn	112
63.74	1.46	4.16	0.47	5.83	Sn	400
65.21	1.431	3.65	0.09	0.99	Sn	321
72.345	1.306	11.56	0.177	6.08	Sn	420
73.165	1.294	6.57	0.315	6.14	Sn	411
78.258	1.222	6.57	0.315	6.14	Al	311
79.487	1.205	100	0.264	105.97	Sn	312
79.81	1.204	62.4	0.168	42.08	Sn	312
89.494	1.094	2.29	0.576	5.29	Sn	431
97.53	1.024	1.99	0.09	0.54	Sn	521

Table 2:- lattice parameters (a and c), unit cell volume (V) and crystal size (τ) of β-Sn in used alloys

Alloys	τ (Å)	a (Å)	c (Å)	V (Å^3)
$Sn_{70}Al_{20}Bi_5Zn_3Cu_2$	443.154	5.866	3.182	109.506
$Sn_{65}Al_{20}Sb_5Pb_5Cd_5$	413.122	5.854	3.179	108.942
$Sn_{70}Al_{20}Sb_5Ag_3Zn_2$	378.257	5.84	3.174	108.247
$Sn_{63}Al_{20}Sb_{10}Pb_5Zn_2$	465.364	5.841	3.179	108.469

Table 3:- lattice microstrain induced in used alloys

Alloys	Lattice strain (ε) $x10^{-3}$
$Sn_{80}Al_{20}$	1.5
$Sn_{70}Al_{20}Bi_5Zn_3Cu_2$	0.3
$Sn_{65}Al_{20}Sb_5Pb_5Cd_5$	0.6
$Sn_{70}Al_{20}Sb_5Ag_3Zn_2$	1.3
$Sn_{63}Al_{20}Sb_{10}Pb_5Zn_2$	9

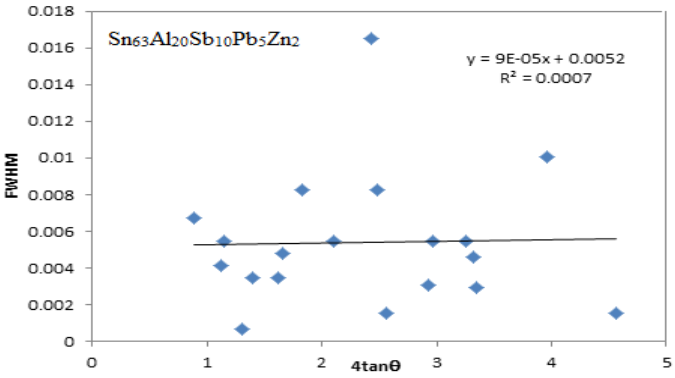

Figure 2 :- FWHM versus 4tanθ for used alloys

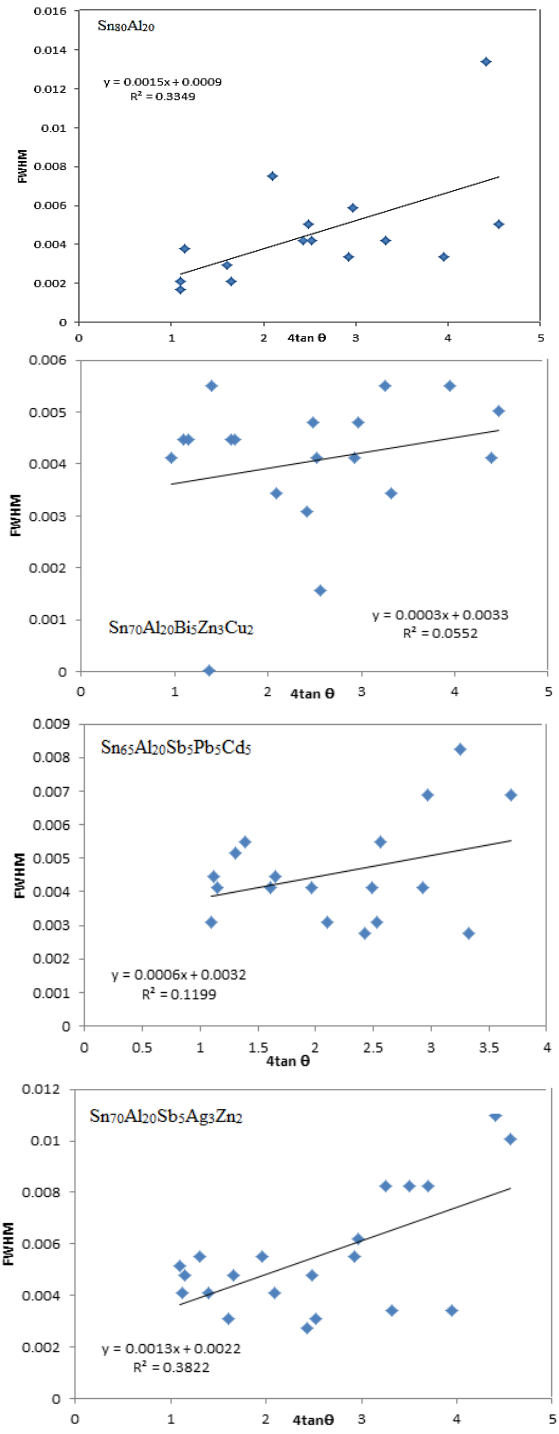

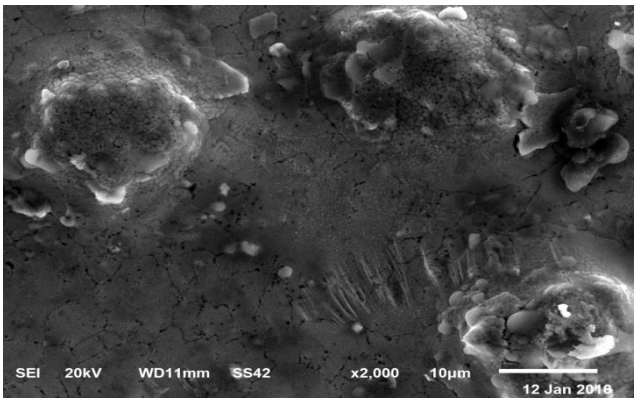

Figure 3a :- SEM of $Sn_{70}Al_{20}Bi_5Zn_3Cu_2$ alloy

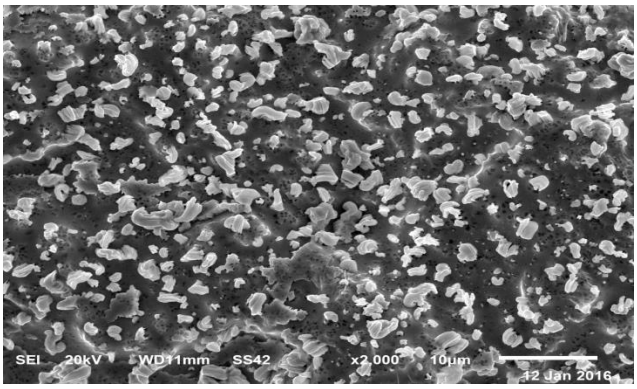

Figure 3b :- SEM of $Sn_{65}Al_{20}Sb_5Pb_5Cd_5$ alloy

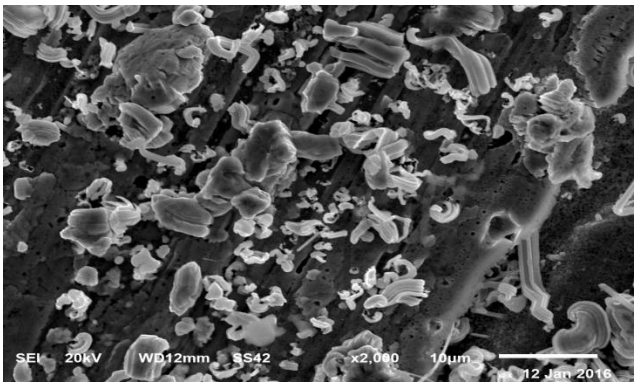

Figure 3c :- SEM of $Sn_{70}Al_{20}Sb_5Ag_3Zn_2$ alloy

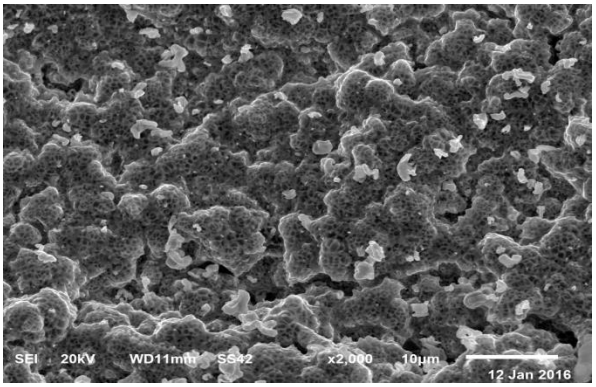

Figure 3d:- of $Sn_{63}Al_{20}Sb_{10}Pb_5Zn_2$ alloy

B. Mechanical properties

Elastic Moduli

The elastic constants are directly related to atomic bonding. The measured elastic modulus of $Sn_{80}Al_{20}$, $Sn_{70}Al_{20}Bi_5Zn_3Cu_2$, $Sn_{65}Al_{20}Sb_5Pb_5Cd_5$, $Sn_{70}Al_{20}Sb_5Ag_3Zn_2$, and $Sn_{63}Al_{20}Sb_{10}Pb_5Zn_2$ alloys are shown in Table 4. Elastic modulus of $Sn_{80}Al_{20}$ alloy varied after Bi- Zn- Cu or Sb- Pb- Cd or Sb- Ag- Zn or Sb- Pb- Zn elements. That is meant, the dissolved different alloying atoms in $Sn_{80}Al_{20}$ matrix formed a solid solution\ or stick on grain boundary/ or formed a small cluster caused variation bond matrix strengthens. The $Sn_{70}Al_{20}Sb_5Ag_3Zn_2$ alloy has adequate elastic modulus value.

Table 4:- elastic modului of used alloys

Alloys	E (GPa)	µ (GPa)	B (GPa)
$Sn_{80}Al_{20}$	39.87	14.68	46.79
$Sn_{70}Al_{20}Bi_5Zn_3Cu_2$	22.99	8.48	26.42
$Sn_{65}Al_{20}Sb_5Pb_5Cd_5$	25.82	9.53	29.68
$Sn_{70}Al_{20}Sb_5Ag_3Zn_2$	34.23	12.64	39.07
$Sn_{63}Al_{20}Sb_{10}Pb_5Zn_2$	44.01	16.25	50.27

Internal Friction and Thermal Diffusivity

Internal friction is a useful tool for the study of structural features of alloys. Resonance curves of $Sn_{80}Al_{20}$, $Sn_{70}Al_{20}Bi_5Zn_3Cu_2$, $Sn_{65}Al_{20}Sb_5Pb_5Cd_5$, $Sn_{70}Al_{20}Sb_5Ag_3Zn_2$ and $Sn_{63}Al_{20}Sb_{10}Pb_5Zn_2$ alloys are shown in Figure 4 and the calculated internal friction values are presented in Table 5. Also from resonance frequency at which the peak damping occur using the dynamic resonance method the thermal diffusivity value was calculated and then listed in Table 5. Internal friction of $Sn_{80}Al_{20}$ alloy deceased after Bi- Zn- Cu or Sb- Pb- Cd or Sb- Ag- Zn or Sb- Pb- Zn elements. The $Sn_{70}Al_{20}Sb_5Ag_3Zn_2$ alloy has lowest internal friction and thermal diffusivity values.

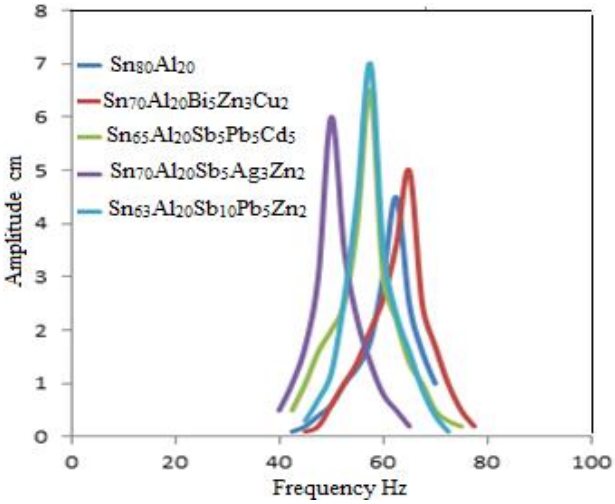

Figure 4:- resonance curves of used alloys

Table 5 :- internal friction and thermal diffusivity of used alloys

Alloys	$Q^{-1} \times 10^{-3}$	$D_{th} \times 10^{-8}$ (m^2/sec)
$Sn_{80}Al_{20}$	18.37	11.58
$Sn_{70}Al_{20}Bi_5Zn_3Cu_2$	16.16	12.58
$Sn_{65}Al_{20}Sb_5Pb_5Cd_5$	9.65	9.27
$Sn_{70}Al_{20}Sb_5Ag_3Zn_2$	6.56	4.71
$Sn_{63}Al_{20}Sb_{10}Pb_5Zn_2$	14.76	7.83

Vickers microhardness and maximum shear stress

The hardness is the property of material, which gives it the capability to resist being enduringly deformed when a load is applied. The Vickers hardness of $Sn_{80}Al_{20}$, $Sn_{70}Al_{20}Bi_5Zn_3Cu_2$, $Sn_{65}Al_{20}Sb_5Pb_5Cd_5$, $Sn_{70}Al_{20}Sb_5Ag_3Zn_2$ and $Sn_{63}Al_{20}Sb_{10}Pb_5Zn_2$ alloys at 10 gram force and indentation time 5 sec are listed in Table 6. Vickers hardness of $Sn_{80}Al_{20}$ alloy varied after adding Bi- Zn- Cu or Sb- Pb- Cd or Sb- Ag- Zn or Sb- Pb- Zn elements. That is because the dissolved different alloying atoms formed a solid solution\ or stick on grain boundary/ or a small cluster effected bonding strengthens. Also the maximum shear stress (μ_m) value of $Sn_{80}Al_{20}$,

$Sn_{70}Al_{20}Bi_5Zn_3Cu_2$, $Sn_{65}Al_{20}Sb_5Pb_5Cd_5$, $Sn_{70}Al_{20}Sb_5Ag_3Zn_2$ and $Sn_{63}Al_{20}Sb_{10}Pb_5Zn_2$ alloys was calculated using the equation [19] and then listed in Table 6.

Table 6 :- Vickers hardness and minimum shear stress of used alloys

Alloys	H_v kg/mm^2	μ_n kg/mm^2
$Sn_{80}Al_{20}$	36.43±2.7	12.01
$Sn_{70}Al_{20}Bi_5Zn_3Cu_2$	30.86±4.12	10.18
$Sn_{65}Al_{20}Sb_5Pb_5Cd_5$	55.7±5.66	18.38
$Sn_{70}Al_{20}Sb_5Ag_3Zn_2$	44.8±5.49	14.78
$Sn_{63}Al_{20}Sb_{10}Pb_5Zn_2$	44.33±7.5	14.63

C. Thermal performance

Thermal analysis is often used to study solid state transformations as well as solid- liquid reactions. The magnitudes of thermal properties depend on the nature of solid phase and on its temperature. The solidus temperature has been reached the tangent line, drawn in by the DSC, is an approximation of the solidus temperature. The liquidus temperature is defined as the temperature at which the graph returns to the baseline. The end of the deviation signifies the end of the phase change. Figure 5 shows the DSC thermographs of $Sn_{70}Al_{20}Bi_5Zn_3Cu_2$, $Sn_{65}Al_{20}Sb_5Pb_5Cd_5$, $Sn_{70}Al_{20}Sb_5Ag_3Zn_2$, and $Sn_{63}Al_{20}Sb_{10}Pb_5Zn_2$ alloys. There is a variation caused in thermo-graph of $Sn_{80}Al_{20}$ alloy after adding Bi- Zn- Cu or Sb- Pb- Cd or Sb- Ag- Zn or Sb- Pb- Zn elements. That is indicated to a change was happen in structure of $Sn_{80}A_{l20}$ alloy and that agrees with the results seen in x-ray diffraction analysis.

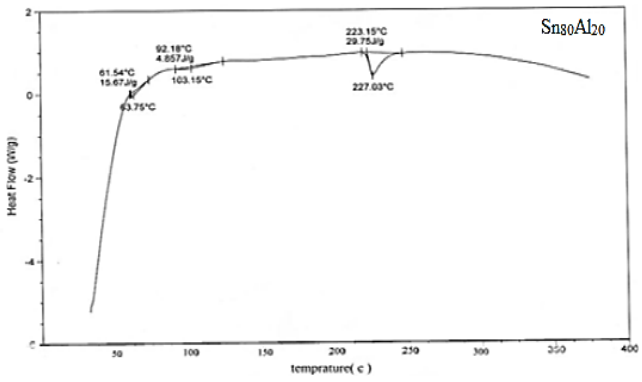

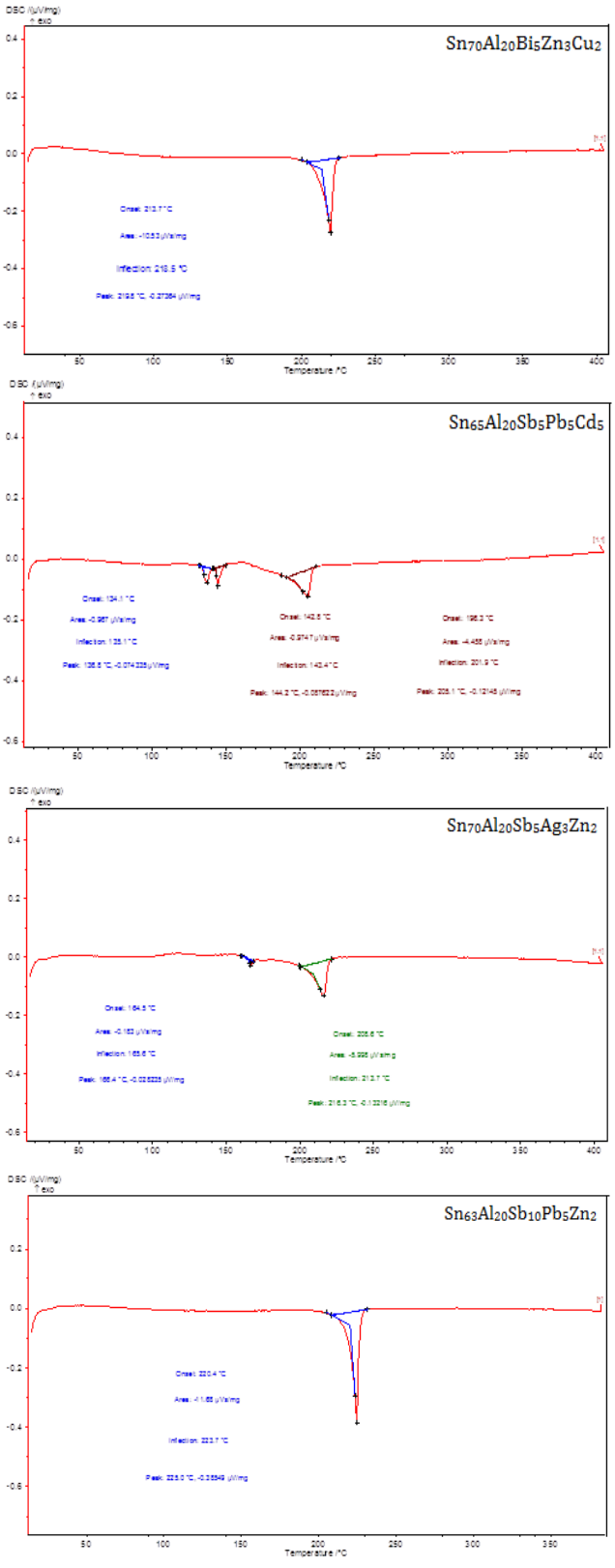

Figure 5 :- DSC thermographs of used alloys

D. Electrochemical Corrosion Behavior

Figure 6 shows the electrochemical polarization curves of $Sn_{80}Al_{20}$, $Sn_{70}Al_{20}Bi_5Zn_3Cu_2$, $Sn_{65}Al_{20}Sb_5Pb_5Cd_5$,

$Sn_{70}Al_{20}Sb_5Ag_3Zn_2$ and $Sn_{63}Al_{20}Sb_{10}Pb_5Zn_2$ alloys in 0. 5 M HCl. The corrosion potential of the $Sn_{80}Al_{20}$, $Sn_{70}Al_{20}Bi_5Zn_3Cu_2$, $Sn_{65}Al_{20}Sb_5Pb_5Cd_5$, $Sn_{70}Al_{20}Sb_5Ag_3Zn_2$ and $Sn_{63}Al_{20}Sb_{10}Pb_5Zn_2$ alloys showed a negative potential. Also the cathodic and the anodic polarization curves exhibited similar corrosion trends. The corrosion potential (E_{Corr}), corrosion current (I_{Corr}), and corrosion rate (C. R) of $Sn_{80}Al_{20}$, $Sn_{70}Al_{20}Bi_5Zn_3Cu_2$, $Sn_{65}Al_{20}Sb_5Pb_5Cd_5$, $Sn_{70}Al_{20}Sb_5Ag_3Zn_2$ and $Sn_{63}Al_{20}Sb_{10}Pb_5Zn_2$ alloys are presented in Table 7. The corrosion rate of $Sn_{80}Al_{20}$ alloy in 0.5 M HCl increased after adding Bi- Zn-Cu or Sb- Ag- Zn or Sb- Pb- Zn elements but it's decreased after Sb-Pb-Cd elements.

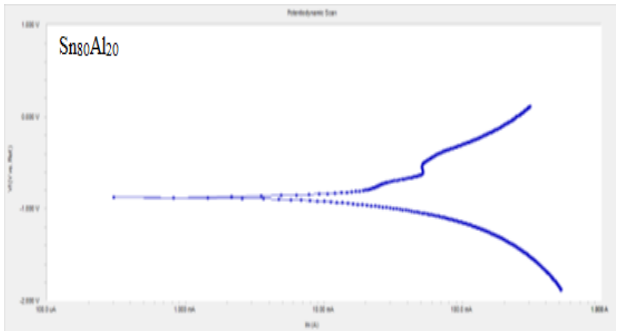

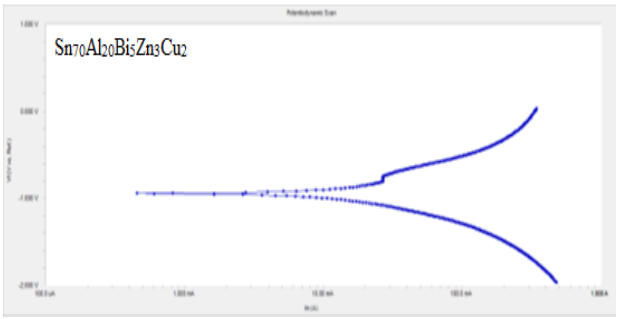

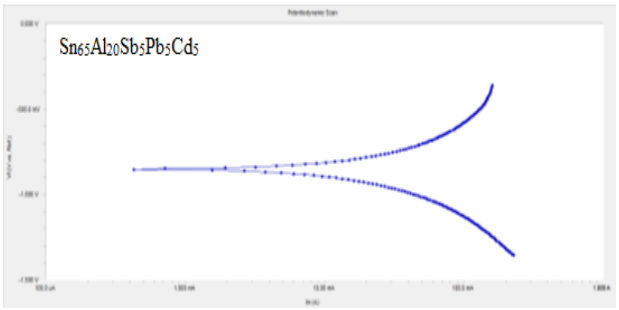

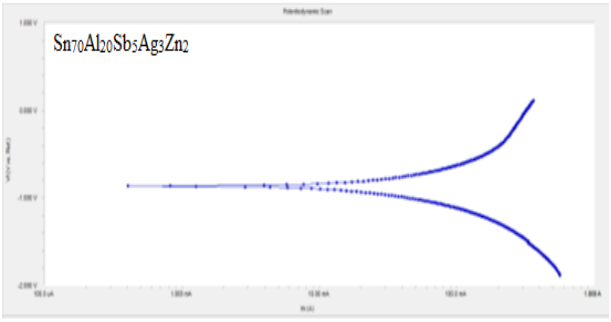

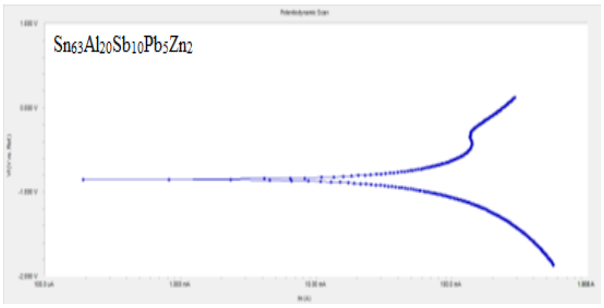

Figure 6 :- electrochemical polarization curves of used alloys

Table 7:- corrosion potential (E_{Corr}), corrosion current (I_{Corr}), and corrosion rate (C. R) of used alloys

Alloys	I_{Corr} $\mu A\ cm^{-2}$	E_{Corr} mV	C. R mpy
$Sn_{80}Al_{20}$	22.60	-876	23.69e3
$Sn_{70}Al_{20}Bi_5Zn_3Cu_2$	23.20	-943	24.32e3
$Sn_{65}Al_{20}Sb_5Pb_5Cd_5$	11.10	-851	11.64e3
$Sn_{70}Al_{20}Sb_5Ag_3Zn_2$	32.20	-863	33.75e3
$Sn_{63}Al_{20}Sb_{10}Pb_5Zn_2$	118.0	-850	123.6e3

EFM is a non-destructive corrosion measurement technique. In which current responses due to a potential perturbation by one or more sine waves are measured at more frequencies than the frequency of the applied signal. The results of EFM experiments are a spectrum of current response as a function of frequency. The intermodulation spectrum of $Sn_{80}Al_{20}$, $Sn_{70}Al_{20}Bi_5Zn_3Cu_2$, $Sn_{65}Al_{20}Sb_5Pb_5Cd_5$, $Sn_{70}Al_{20}Sb_5Ag_3Zn_2$ and $Sn_{63}Al_{20}Sb_{10}Pb_5Zn_2$ alloys in 0. 5 M HCl solutions are shown in Figure 7. The larger peaks were used to calculate the corrosion current density (icorr) and the corrosion rate (C. R) whish listed in Table 8. The corrosion current density (icorr) of $Sn_{80}Al_{20}$ alloy in 0.5 M HCl increased after adding Bi- Zn-Cu or Sb- Pb-

Cd or Sb- Pb- Zn elements but it's decreased after Sb-Ag-Zn elements.

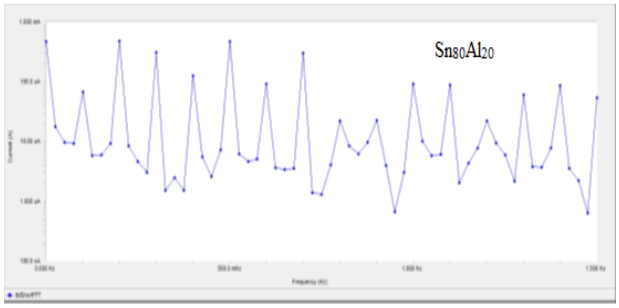

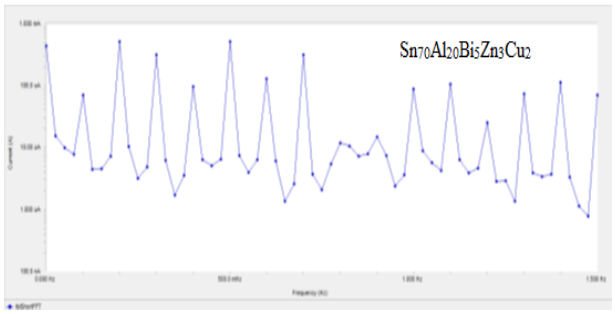

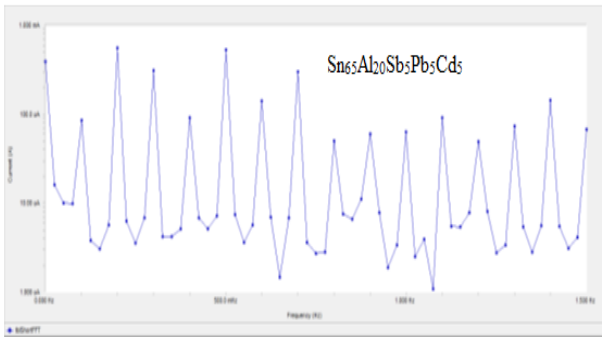

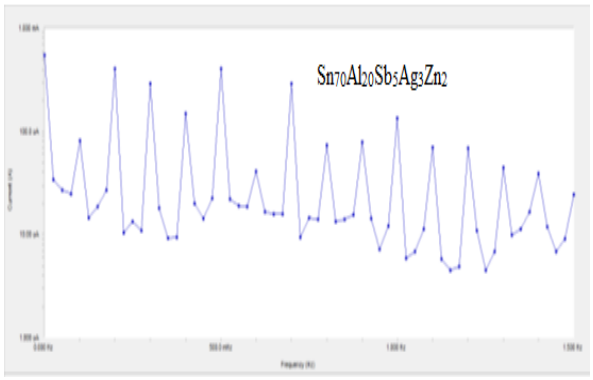

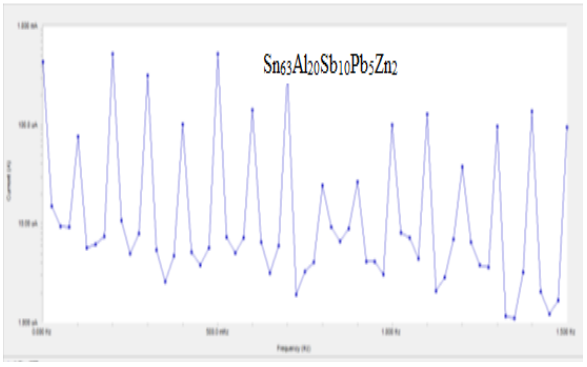

Figure 7:- intermodulation spectrum obtained by EFM technique for used alloys

Table 8:- the corrosion current density (icorr) and the corrosion rate (C. R) of used alloys

Alloys	i_{Corr} µA cm^{-2}	C. R mpy
$Sn_{80}Al_{20}$	371.2	388.6
$Sn_{70}Al_{20}Bi_5Zn_3Cu_2$	419.0	438.7
$Sn_{65}Al_{20}Sb_5Pb_5Cd_5$	483.8	506.5
$Sn_{70}Al_{20}Sb_5Ag_3Zn_2$	287.4	301.0
$Sn_{63}Al_{20}Sb_{10}Pb_5Zn_2$	418.2	437.8

IV. CONCLUSION

1. Microstructural of $Sn_{80}Al_{20}$ alloy changed after adding different ternary alloying elements, Bi- Zn-Cu or Sb- Pb- Cd or Sb- Ag- Zn or Sb- Pb- Zn.
2. Internal friction of $Sn_{80}Al_{20}$ alloy deceased after Bi-Zn- Cu or Sb- Pb- Cd or Sb- Ag- Zn or Sb- Pb- Zn elements. The $Sn_{70}Al_{20}Sb_5Ag_3Zn_2$ alloy has lowest internal friction and thermal diffusivity values.
3. Elastic modulus and Vickers hardness of $Sn_{80}Al_{20}$ alloy varied after Bi- Zn- Cu or Sb- Pb- Cd or Sb-Ag- Zn or Sb- Pb- Zn elements. The $Sn_{70}Al_{20}Sb_5Ag_3Zn_2$ alloy has adequate elastic modulus and Vickers hardness values.
4. The corrosion current density (icorr) of $Sn_{80}Al_{20}$ alloy in 0.5 M HCl increased after adding Bi- Zn-Cu or Sb- Pb- Cd or Sb- Pb- Zn elements but it's decreased after Sb-Ag-Zn elements
5. The corrosion rate of $Sn_{80}Al_{20}$ alloy in 0.5 M HCl increased after adding Bi- Zn-Cu or Sb- Ag- Zn or Sb- Pb- Zn elements but it's decreased after Sb-Pb-Cd elements

V. REFERENCES

[1] A. Zeren, E. Feyzullahoglu, M. Zeren, Materials and Design 28 (2007) 318

[2] P G Forrester, Met. Rev. 5 (1960) 507

[3] G C Pratt G C, Int. Met. Rev. 18 (1973) 62

[4] W I M Tegart, Elements of mechanical metallurgy. New York: The MacMillan Co. 1966: 91

[5] P G Forrester, Curr. Engg. Pract. 3 (1961) 4

[6] T. Desaki, Y. Goto, S. Kamiya, JSAE Rev. 21 (2000) 321

[7] K. Lepper, M. James, J. Chashechkina, D.A. Rigney, Wear 203–204 (1997) 46

[8] J P Pathak and S Mohan, Bull. Mater. Sci. 26: 3 (2003) 315

[9] A. A. El-Daly, Y. Swilem, A.E. Hammad, J. Alloy. Comp. 471 (2009) 98

[10] M.J. Esfandyarpour, R. Mahmudi, Mater. Sci. Eng. A 530 (2011) 402–410

[11] A. El-Bediwi, A.R. Lashin, M. Mossa, M. Kamal, Mater. Sci. Eng. A 528 (2011) 3568

[12] A. B. El-Bediwi, Radia. Eff. Def. Solid. 159 (2004) 125

[13] A. B. El-Bediwi, Radia. Eff. Def. Solid. 159 (2004) 539

[14] M.J. Esfandyarpour, R. Mahmudi, Mater. Sci. Eng. A 530 (2011) 402

[15] M. Kamal, A. El-Bediwi and M. R. El-Shobaki, Radia. Eff. Def. Sol. 161 (2006) 549

[16] B. D Cullity, "Element of x-ray diffraction" Ch.10 (1959) 297

[17] S. Sppinert and W. E. Teffit, ASTM, Proc. 61 (1961) 1221

[18] E. Schreiber, O. L. Anderson and N. Soga, Elastic Constants and their Measurement, McGraw-Hill Book Company, Ch. 4 (1973)

[19] S. Timoshenko and J. N. Goddier, "Theory of elasticity, 2nd Ed", McGraw-Hill, New York, (1951) 277